



An “imaging-biopsy” strategy for colorectal tumor reconfirmation by multipurpose paramagnetic quantum dots



Xiaohong Xing^a, Bingbo Zhang^{b,*}, Xiaohui Wang^a, Fengjun Liu^a, Donglu Shi^{b,c},
Yingsheng Cheng^{d,*}

^a Department of Radiology of the Tenth People's Hospital, Tongji University School of Medicine, Shanghai, 200072, PR China

^b Shanghai East Hospital, The Institute for Biomedical Engineering & Nano Science, Tongji University School of Medicine, Shanghai, 200120, PR China

^c The Materials Science and Engineering Program, Dept of Mechanical and Materials Engineering, University of Cincinnati, Cincinnati, OH, 45221-0072, USA

^d Department of Radiology, Shanghai Sixth People's Hospital, Shanghai Jiaotong University, Shanghai, 200233, PR China

ARTICLE INFO

Article history:

Received 25 August 2014

Accepted 20 January 2015

Available online 7 February 2015

Keywords:

Quantum dots
Colorectal cancer
Molecular imaging
Biopsy
MRI

ABSTRACT

Glucose transporter1 (Glut1) plays important roles in treatment of colorectal cancer (CRC) involving early-stage diagnosis, subtype, TNM stage, and therapeutic schedule. Currently, *in situ* marking and tracking of the tumor biomarkers *via* clinical imaging remains great challenges in early stage CRC diagnosis. In this study, we have developed a unique cell-targeted, paramagnetic-fluorescent double-signal molecular nanoprobe for CRC *in vivo* magnetic resonance imaging (MRI) diagnosis and subsequent biopsy. The unique molecular nanoprobe is composed of a fluorescent quantum dot (QD) core; a coating layer of paramagnetic DTPA-Gd coupled BSA (^{Gd}DTPA-BSA), and a surface targeting moiety of anti-Glut1 polyclonal antibody. The engineered ^{Gd}DTPA-BSA@QDs-PcAb is 35 nm in diameter and colloidal stable under both basic and acidic conditions. It exhibits strong fluorescent intensities and high relaxivity (r_1 and r_2 : 16.561 and 27.702 s⁻¹ per mM of Gd³⁺). Distribution and expression of Glut1 of CRC cells are investigated by *in vitro* cellular confocal fluorescent imaging and MR scanning upon treating with the ^{Gd}DTPA-BSA@QDs-PcAb nanoprobe. *In vivo* MRI shows real-time imaging of CRC tumor on nude mice after intravenously injection of the ^{Gd}DTPA-BSA@QDs-PcAb nanoprobe. *Ex vivo* biopsy is subsequently conducted for expression of Glut1 on tumor tissues. These nanoprobe are found biocompatible *in vitro* and *in vivo*. ^{Gd}DTPA-BSA@QDs-PcAb targeted nanoprobe is shown to be a promising agent for CRC cancer *in vivo* MRI diagnosis and *ex vivo* biopsy analysis. The “imaging-biopsy” is a viable strategy for tumor reconfirmation with improved diagnostic accuracy and biopsy in personalized treatment.

© 2015 Elsevier Ltd. All rights reserved.

1. Introduction

Colorectal cancer (CRC) is the third most commonly diagnosed cancer in males and second in females, with over 1 million new cancer cases and 0.5 million deaths estimated to have occurred each year [1]. The stage where CRC is detected determines patients outcome, with 5-year survival rates of more than 90% for stage I disease and less than 10% for stage IV [2]. High CRC death rates can be significantly reduced by improved treatment and early detection.

Tumor markers differ from normal cells and rapidly emerge in tumor progression *via* angiogenesis, tumor cellularity, metabolism, and oxygenation which is closely related to cancer pathogenesis, invasion and metastasis [3–5]. Therefore, cancer biomarkers can be used in establishing specific diagnosis and disease prognosis. The glucose transporters1 (Glut1), as a cell surface protein with extracellular domains, has been confirmed to express a significant number of malignant tumors, including CRC, based on the immunohistochemistry (IHC) studies. Younes reported a high level of a Glut1 expression that was closely associated with an incidence of lymph node metastases in CRC [6]. Haber assessed Glut1 immunostaining in colorectal carcinoma to identify patients with poorer prognosis [7]. Sakashita suggested that Glut1 expression was positive in 18% of low-grade adenomas and in 63% of high-grade adenomas [8]. Wincewicz detected positive 58.3% Glut1 expression in

* Corresponding authors. Tel.: +86 21 65983706 819; fax: +86 21 65983706 0.
E-mail addresses: bingbozhang@tongji.edu.cn (B. Zhang), cjr.chengysh@vip.163.com (Y. Cheng).

colorectal adenocarcinoma, while no expression in normal colorectal tissue [9]. Fenske found Glut1 expression related to potential malignant and predictor of poor prognosis [10]. These studies suggested that imaging of expression levels of Glut1 can provide an important basis for the tumor stage, tumor invasiveness and histological differentiation in order to establish personalized treatment of CRC patients.

MRI is a powerful noninvasive medical tool for tumor diagnosis with impressive anatomic resolution and tissue penetration, but it is limited by low sensitivity and cell specificity [11]. Clinical MRI contrast agents (CAs) include Gd (III) chelates, e.g., Gd-DTPA-BMA, Gd-DOTA, and other small molecular Gd-based CAs. Their structures are stable, but with poor relaxivity, specificity, and retention time in blood stream [12,13]. A promising solution to improving MRI sensitivity and specificity can be achieved by conjugation specific CAs with anti-tumor biomarker antibodies. Upon administration of these specific CAs, biomarker expression levels and distribution of the diseased tissues on CRC tumor can be effectively tracked by the targeted and CAs-enhanced imaging techniques [14]. It should be noted that in clinical cancer diagnosis the suspicious lesion tissues in MRI are often removed for conclusive diagnosis using the immunohistochemical (IHC) analysis [8,15]. It is also used to identify the tumor type, degree of malignancy, metastasis and recurrence [6,16]. There is, therefore, a great need to search for multipurpose tumor-specific CAs with MRI moieties and tissue molecular profiling moieties.

In this study, integrated gadolinium (Gd) -functionalized quantum dots (Gd^{III} -DTPA-BSA@QDs) were designed and synthesized as MRI CAs and IHC signal reporter. Gd^{III} -DTPA-BSA, a paramagnetic metal ion biomolecular complex, was used as a moiety of T_1 -weighted MRI CAs and the reaction sites for conjugation of targeting ligands such as peptides, antibodies, and DNA. QDs were used as moieties of fluorescent reporters in IHC for tissue biopsy. QDs have uniform size and shape, narrow emission peak, high quantum yield (QY), and photo and chemical stability [17–19]. Due to their special properties, QDs have been widely used as nanoprobes for biomedical labeling such as *in vitro* cancer molecular pathology [20,21]. As fluorescent probes for immunohistochemistry assay, QDs have significant advantages over conventional fluorophores [21]. High quality core/shell semiconductor QDs were synthesized in this study following a previously reported hot-injection method [22,23].

Gd^{III} -DTPA-BSA was prepared by conjugation of BSA and diethylenetriaminepentaacetic dianhydride (DTPAA), and chelation with Gd^{3+} . For integration of two imaging moieties, hydrophobic QDs were surface engineered from organic to the aqueous phase in the presence of Gd^{III} -DTPA-BSA aqueous solution under ultrasonication [24]. The as-prepared Gd^{III} -DTPA-BSA@QDs exhibited good water-dispersibility, high relaxivity and strong anti nonspecific binding. Upon conjugation with anti-tumor polyclonal antibody (Glut1) [25], the resulting Gd^{III} -DTPA-BSA@QDs-PcAb were investigated for *in vitro* and *in vivo* tumor targeted imaging. Furthermore, the expression and distribution of Glut1 on tumor site was investigated in tissue biopsy with the fluorescent reporter of Gd^{III} -DTPA-BSA@QDs-PcAb.

2. Materials and methods

2.1. Materials

2.1.1. Reagents and materials

Cadmium oxide (99.99%), selenium powder (99.99%), zinc oxide (ZnO, 99.99%), sulfur (99.98%), octadecylamine (ODA, 90%), oleic acid (OA, 90%), 1-octadecene (ODE, 90%), tri-n-octylphosphine oxide (TOPO, 90%) and 1-ethyl-3-(3-dimethylaminopropyl) carbodiimide hydrochloride (EDC•HCl) were purchased from Sigma–Aldrich. Diethylenetriaminepentaacetic acid dianhydride (DTPAA, 95%), dimethyl sulfoxide (99.8%), gadolinium (III) chloride hexahydrate (99.9%) were purchased from Alfa Aesar. Glut1 antibody was purchased from Millipore

Corporation. Bovine serum albumin (BSA) was purchased from Beijing Dingguo Biotechnology. Trisodium citrate dehydrate, trichloromethane, acetone, sodium hydrogen carbonate, argon was purchased from local suppliers. Deionized water (18.2 M Ω cm resistivity at 25 °C) was used in this study. All the chemicals were used without further purification.

2.2. Methods

2.2.1. Preparation of hydrophobic surfactant-capped core/shell QDs

Hydrophobic surfactant-capped QDs were synthesized with minor modifications according to previously published procedures [22,23]. The CdSe core synthesis was carried out as follows. Separately, CdO (0.6 mmol), OA (0.8 mL) and ODE (8 mL) were heated to 150 °C in an argon atmosphere in a three-necked flask. After dissolution of CdO, the solution was cooled to room temperature, followed by adding TOPO (1 g) and ODA (2.5 g), and the mixture was heated again to 260 °C. At this temperature, a stock solution (3.6 mmol of Se powder dissolved in 2 mL of TOP) was rapidly injected into the reaction chamber (containing a Cd precursor) to start nucleation until the color change to red. Addition of ethanol into the solution resulted in a precipitate which was washed with acetone for several times and then dried for use.

Core/shell QDs were synthesized as follows. CdSe nanocrystals dissolved in 10 mL of hexane were mixed with 1.5 g of ODA and 5.0 g of ODE in a 25 mL three-neck flask. The flask was then pumped down at room temperature with argon atmosphere for 30 min to remove air at 100 °C for another 5–10 min to remove hexane from the system. Subsequently, the system was switched to argon flow and the reaction mixture was further heated to 240 °C for injections of Cd, Zn and S resource solution using the method described by Li [26]. After reaction, the raw products were separated by acetone precipitation followed by centrifugation. In this study, CdSe/CdS^{2ML}/Cd_{0.75}Zn_{0.25}S/Cd_{0.5}Zn_{0.5}S/Cd_{0.25}Zn_{0.75}S/ZnS^{2ML} core/shell QDs were provided for further experiment. Herein, ML is the abbreviation of monomolecular layer.

2.2.2. Preparation of Gd^{III} -DTPA-BSA complex

The synthesis of Gd^{III} -DTPA-BSA complex was according to a previously published protocol with minor modifications [27]. Briefly, 5 g of BSA was dissolved in 75 mL of 0.1 M NaHCO₃ (pH 8.5) solution. 5 g of DTPAA dissolved in 25 mL of dry DMSO was then added to the BSA solution. The pH value of mixture solution was adjusted to 8.5 by using 1 M NaOH. The solution was stirred for 2 h at room temperature and dialyzed against 5 × 4 L of deionized water. Subsequently, 2.5 g of GdCl₃·6H₂O was dissolved in 25 mL of 0.1 M Na-acetate buffer (pH 6.0) and added drop wise to the above BSA-DTPA solution to produce Gd^{III} -DTPA-BSA complex, while keeping pH at 6.5. The solution was further stirred for 24 h at room temperature. Redundant Gd^{3+} were removed through dialyzing Gd^{III} -DTPA-BSA against 5 × 4 L of citrate buffer (0.1 M, pH 6.5) and 5 × 4 L of deionized water. Finally, the solution of Gd^{III} -DTPA-BSA was frozen-dry from liquid to solid for further use.

2.2.3. Preparation of Gd^{III} -DTPA-BSA@QDs

The hydrophilic Gd^{III} -DTPA-BSA-coated QDs was synthesized according to our previously reported procedure [24]. Core/shell QDs/chloroform solution was transferred into a clean syringe for injection. The mole ratio of Gd^{III} -DTPA-BSA to QDs was kept at 500. Typically, the weighted Gd^{III} -DTPA-BSA (30 mg) was completely dissolved in 4 mL of deionized water in a 10 mL beaker. The beaker was placed under an ultrasonic cell crusher with an ultrasonic booster. The top of the booster was ~0.5 cm lower than the liquid level of Gd^{III} -DTPA-BSA water solution. The top of the long syringe needle was placed next to that of the booster. The QDs/chloroform solution was slowly injected into the Gd^{III} -DTPA-BSA water solution with ultrasonication at 300–500 W pulsed every 10 s for an interval of 10 s. The emulsion-like solution was treated by a rotary evaporator to remove chloroform. In the last step, Gd^{III} -DTPA-BSA@QDs were purified by ultracentrifugation at 100,000 × g for 15 min to remove the remains of Gd^{III} -DTPA-BSA. The purified product was dispersed in borate saline buffer (50 mM, pH 8.2) and stored at 4 °C for further study.

2.2.4. Preparation of targeted dual-signal Gd^{III} -DTPA-BSA@QDs-PcAb nanoprobes

Gd^{III} -DTPA-BSA@QDs were conjugated with antibodies by using EDC-HCl as the cross-linker. The dual-signal Gd^{III} -DTPA-BSA@QDs were reacted with antibodies at a QDs/Glut1PcAb/EDC-HCl molar ratio of 1:10:4000 in borate saline buffer (50 mM, pH 8.2) with continuously stirring for 2 h at room temperature. The final bioconjugates were dispersed in phosphate buffered saline (PBS, 0.01 M, pH 7.4, 0.5% BSA, 0.02% sodium azide) after purifying by ultracentrifugation at 100,000 × g for 15 min and washed with 0.01 M PBS (pH 7.4) twice.

2.2.5. *In vitro* relaxation rate and MRI

The longitudinal and transverse relaxation times of Gd^{III} -DTPA-BSA and Gd^{III} -DTPA-BSA@QDs were determined by using the 1.41 T minispec mq 60 NMR analyzer (Bruker, Germany) at 37 °C. The relaxivity values of r_1 and r_2 were calculated by fitting the $1/T_1$ and $1/T_2$ relaxation time (s^{-1}) versus Gd^{3+} concentration (mM) curves. The *in vitro* MR images of the Gd^{III} -DTPA-BSA@QDs samples were obtained using a MRI system (MesoMR23-060H-I; Shanghai Niumag Corporation, China). The measurement conditions were as follows: T_1 -weighted sequence; multi-

slice spin echo; repetition time/echo time (TR/TE) = 1150/11.5 ms; matrix acquisition = 256×192 ; number of excitations (NEX) = 8; field of view (FOV) = 80 mm \times 80 mm; FOV phase of 40%; thickness = 5.0 mm; 0.5 T, and 32 °C.

2.2.6. Cytotoxicity study of Gd^{3+} DTPA-BSA@QDs

The cytotoxicity of Gd^{3+} DTPA-BSA@QDs against 3T3 cells was studied using the MTT colorimetric procedure. Cells were seeded at a density of 5×10^3 cells/well in 96-well flat-bottomed plates, and allowed to adhere overnight. The cells were washed twice with PBS and incubated with Gd^{3+} DTPA-BSA@QDs at different Gd^{3+} concentrations for 24, 48, and 72 h. Next, the cells were washed twice with PBS and fresh culture medium was added. 20 μ L of MTT solution (5 mg/mL in PBS) was then added to each well and the cells were incubated for an additional 4 h at 37 °C. The media were removed and the cells were dissolved in 100 μ L of DMSO. Absorbance at 570 nm was measured with a microplate reader. The data were presented as the percentages of viable cells compared to the survival of a control group with a mean \pm s.e. ($n = 5$).

2.2.7. Cell-targeted bimodal imaging

Confocal laser scanning microscopy (CLSM) imaging (Leica TCS SP5II) and MRI were employed to assess the specific binding capability of prepared Gd^{3+} DTPA-BSA@QDs-PcAb nanoprobes with HCT-116 cells. Cells seeded in a 6-well plate in 2 mL of culturing medium were exposed to a humidified 5% CO_2 atmosphere at 37 °C and cultured for 24 h before adding the nanoprobes. Prior to the experiment, cells were washed twice with PBS to remove the growth medium and then incubated with Gd^{3+} DTPA-BSA@QDs-PcAb or Gd^{3+} DTPA-BSA@QDs for 30 min. The cells were washed twice with PBS and living cell imaging was performed on the confocal laser scanning microscopy.

For *in vitro* cell MRI experiments, the cells were incubated with Glut1-targeted Gd^{3+} DTPA-BSA@QDs-PcAb nanoprobes and non-targeted Gd^{3+} DTPA-BSA@QDs, respectively, at 37 °C for 2 h. Cells were washed and redispersed in 100 μ L of PBS and inserted in a 60 mm diameter MR coil. The *in vitro* MR imaging was performed on the NIUMAG MRI system (NMI20). The measurement conditions were as follows: T₁-weighted sequence; multi-slice spin echo (MSE); TR/TE = 400/5.6 ms; matrix acquisition = 200×128 ; NEX = 8; FOV = 55 mm \times 55 mm; FOV phase: 20%; thickness = 5 mm; 0.5 T, and 32.0 °C. The relaxation times were respectively measured for comparison.

To evaluate the targeting capability of the Gd^{3+} DTPA-BSA@QDs-PcAb nanoprobes, a competitive inhibition cell assay was performed using fluorescent imaging by adding free antibodies (10 μ L, 1 mg/mL) into Glut1-expressed cells for preincubation before introduction of the Glut1-targeted Gd^{3+} DTPA-BSA@QDs-PcAb nanoprobes.

2.2.8. Tumor implantation

All animal experiments were carried out in accordance with guidelines approved by the ethics committee of Tongji university, Shanghai, China. HCT 116 cells (2×10^6) were injected into the right hind leg of female Balb/c nude mice. The subcutaneous tumors with a diameter of 1.0–2.0 cm were ready for MR imaging and IHC analysis after inoculation for 14–18 days.

2.2.9. *In vivo* MRI of Gd^{3+} DTPA-BSA@QDs-PcAb nanoprobes on tumor-bearing mice

In vivo MRI experiments were performed on a 0.5T MRI scanner (MesoMR23-060H-I, NIUMAG, China). To compare the contrast enhancement of targeted and non-targeted nanoprobes on the colorectal tumor-bearing mice, MR images were obtained before and after injection with the Gd^{3+} DTPA-BSA@QDs-PcAb NPs and Gd^{3+} DTPA-BSA@QDs at dosage of 0.05 mmol of Gd^{3+} per kg body weight, respectively. The measurement conditions were as follows: T₁-weighted sequence; multi-slice spin echo; repetition time/echo time (TR/TE) = 1400/18.2 ms, matrix acquisition = 256×192 ; number of excitations (NEX) = 16; field of view (FOV) = 80 mm \times 80 mm; FOV phase of 40%; thickness = 3.5 mm; 0.5 T, and 32 °C.

2.2.10. Tumor tissue biopsy and IHC analysis

Tumor tissues were obtained by needle biopsies and fixed for IHC analysis. In this study, IHC analysis was based on the comparison between an enzyme reporter and the Gd^{3+} DTPA-BSA@QDs-PcAb reporter. For Glut1 staining, the fixed sections from tumor biopsy specimens were divided into two groups. In the enzyme reporter based IHC analysis, the positive group was stained by the Glut1 primary antibody (AB1341, Millipore Corporation) at a 1:100 dilution first for 40 min and followed by HRP- labeled IgG, which was visually observed by Diaminobenzidine plus (DAB Plus) (Biotec Well, Shanghai, China). HRP- labeled IgG was added in the control group instead of Glut1 primary antibody and visually observed by DAB Plus directly. In the nanoprobe reporter based IHC analysis, the positive group was stained by Gd^{3+} DTPA-BSA@QDs-PcAb (25 nM) directly. The control group was stained by Gd^{3+} DTPA-BSA@QDs (25 nM). Both cases were followed by DAPI staining. The Glut1 expression was assessed by immunohistochemical examination using a light microscope and by immunofluorescent examination using CLSM imaging.

2.2.11. *In vivo* toxicity study

Liver, spleen and kidney organs were removed from the anesthetized mice post-injected with the Gd^{3+} DTPA-BSA@QDs nanoprobes after 15 days and fixed, embedded

into paraffin. The fixed organs were sliced, stained with hematoxylin and eosin (H&E), and subjected to optical microscopy study.

2.2.12. Pharmacokinetics of Gd^{3+} DTPA-BSA@QDs

The organs and tissues including liver, spleen, kidney, heart, lung, and intestine were collected from the anesthetized mice post-injected with Gd^{3+} DTPA-BSA@QDs at dosage of 0.05 mmol of Gd^{3+} per kg body weight, and eroded with concentrated nitric acid for disclosing the biodistribution of the particles by ICP-AES at 2 h, 12 h, 24 h, 4 d, 7 d, and 14 d, respectively. Three mice without injection were used as the blank control.

2.2.13. Characterization

The morphology and size of hydrophobic QDs and hydrophilic Gd^{3+} DTPA-BSA@QDs were studied using a DX 2700 transmission electron microscope (TEM). The Fourier transform infrared spectroscopy (FTIR) spectra were obtained on a FT-IR spectrometer (SENSOR 27, BRUKER). The molecular weight of BSA and DTPA-BSA were studied by the matrix-assisted laser desorption/ionization time-of-flight mass spectrometry (MALDI-TOF MS) (AB SCIEX 5800, USA). The hydrodynamic diameters (HDs) of Gd^{3+} DTPA-BSA@QDs in aqueous solution were evaluated using a dynamic light scattering (DLS, NanoZS90, Malvern). The absorbance and emission spectra of hydrophobic QDs in chloroform and Gd^{3+} DTPA-BSA@QDs in deionized water were recorded on a Cary 50 spectrometer and LS-55 spectrophotometer under 470 nm excitation, respectively.

3. Results and discussion

3.1. Synthesis and size characterization of Gd^{3+} DTPA-BSA@QDs

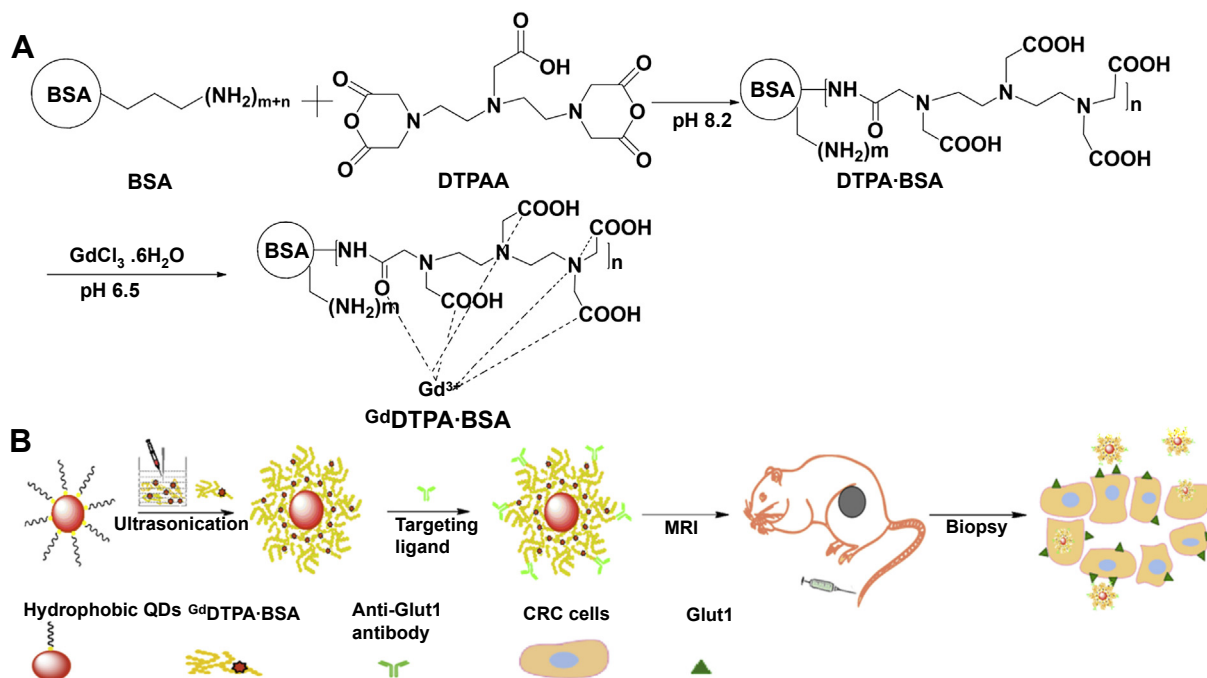
Scheme 1 A illustrates the synthesis route of Gd^{3+} DTPA-BSA complexes. Gd^{3+} DTPA-BSA was synthesized by reaction of cyclic anhydride of DTPA with BSA and subsequent addition of Gd^{3+} ions for chelation. The DTPA groups were covalently bound to the amine moieties of BSA, and the Gd^{3+} was chelated in the DTPA moieties. The successful coupling of DTPA and BSA was confirmed by FTIR analysis.

The FTIR spectrum of BSA, DTPAA and its derivative Gd^{3+} DTPA-BSA were shown in Fig. 1A. A peak at 1444 cm^{-1} in the spectrum of Gd^{3+} DTPA-BSA attributes to the NHCO (amide), which indicates the acylamino bond in Gd^{3+} DTPA-BSA. The strong peaks include O–H, N–H (around 3380 cm^{-1}), and C=O (1738 cm^{-1}) vibrations in the spectra of Gd^{3+} DTPA-BSA (spectrum c). These peaks of DTPAA (spectrum b) appear weak, but can be distinguished from spectrum a, suggesting the incorporation of carboxylate groups into BSA [28].

To further verify DTPA to be attached to BSA, the molecular weights of native BSA and the resulting BSA-DTPA conjugate were characterized by MALDI-TOF mass spectrometer (Fig. 1B). An increase is observed from the peak of 66977.2 Da (the native BSA) to 71005.8 Da (DTPA-BSA). This increase indicates that each BSA macromolecule is coupled with about 10 of DTPA small molecules. This result is consistent with the previous report [29]. The disappearance of the BSA peak in the spectrum of DTPA-BSA suggests the completion of coupling.

Albumin is the most abundant protein in the circulatory system and contributes 80% to colloid osmotic blood pressure. BSA and its derivatives have numerous biochemical applications that include blocking agents in enzyme-linked immunosorbent assay [30], stabilizers in enzymes processing [31], ligands in surface engineering [24,32] and nanocarriers [33–35]. In this study, BSA has two roles, namely the ligands for surface engineering of hydrophobic QDs and nanocarriers for linking Gd^{3+} DTPA and antibodies. Practically, BSA, as a multivalent ligand with abundant free carboxyl, amino and disulfide bonds, has been successfully used in our previous work for surface engineering of nanoparticles [24,32]. In this study, for multipurpose applications, BSA is employed with MRI moiety beforehand, and utilized for water-solubilization of hydrophobic QDs. Gd^{3+} DTPA-BSA is experimentally found to be effective and facile in the phase transfer of QDs under ultrasonication.

Fig. 1C shows the TEM images of the original hydrophobic QDs and its water dispersible counterpart. Gd^{3+} DTPA-BSA@QDs under



Scheme 1. Schematic illustration of the Gd^{3+} -DTPA-BSA@QDs nanoprobe for targeted CRC tumor imaging. (A) Synthesis of Gd^{3+} -DTPA-BSA complexes. (B) Schematic illustration of gadolinium-functionalized QDs-polyclonal antibody bioconjugates for targeted tumor MRI and tissue biopsy.

TEM is uniform in size without obvious aggregates. Furthermore, their corresponding HDs were analyzed for comparison (Fig. 1D). The mean HD of Gd^{3+} -DTPA-BSA@QDs is 35 nm, larger than that of hydrophobic QDs in chloroform (9 nm). This indicates the Gd^{3+} -DTPA-BSA coating on the QDs surfaces. The free carboxyl groups of Gd^{3+} -DTPA-BSA layer on the QDs can allow for coupling antibodies for targeted MRI and tissue biopsy. This basic design principle of experiment is illustrated in Scheme 1B.

3.2. Optical and relaxivity characterization of Gd^{3+} -DTPA-BSA@QDs

The spectroscopic properties of Gd^{3+} -DTPA-BSA@QDs in aqueous phase are nearly identical to those of initial hydrophobic core/shell QDs in organic phase (Fig. 2). They emit sharp and highly symmetrical fluorescence at 680 nm. After ultracentrifugation to remove the supernatant, the precipitated Gd^{3+} -DTPA-BSA@QDs can be readily redispersed in various hydrophilic solvents such as DMEM

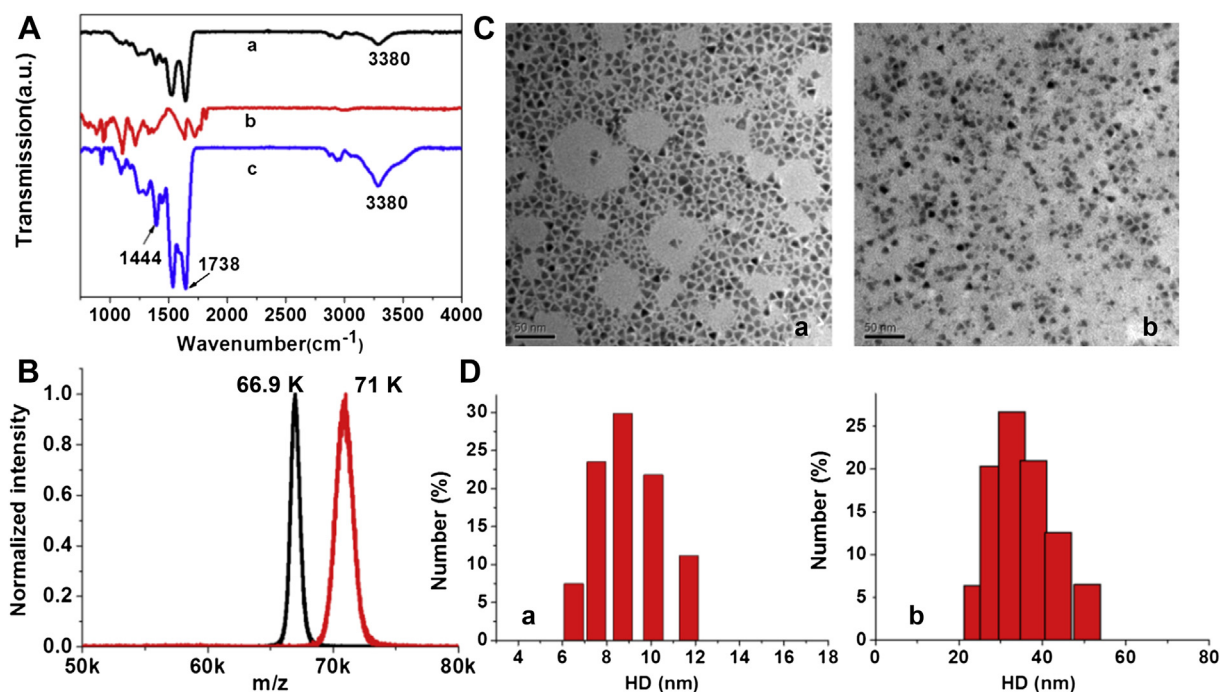


Fig. 1. (A) FTIR spectra of BSA (a), DTPAA (b) and Gd^{3+} -DTPA-BSA (c). (B) MALDI-TOF mass spectra of BSA and DTPA-BSA with sinapinic acid as matrix and water (1/1, v/v) with 0.1% trifluoroacetic acid as cationizing agent. (C) TEM images of hydrophobic QDs (a) and hydrophilic Gd^{3+} -DTPA-BSA@QDs (b). (D) DLS data of hydrophobic QDs in chloroform (a) and Gd^{3+} -DTPA-BSA@QDs in water (b).

without precipitates. Their colloidal stability in cell growth media at different storage times and the optical stability are characterized as shown in Fig. 3. As expected, the Gd^{3+} DTPA·BSA-coated QDs are stable in 7 days showing no signs of sedimentation (Fig. 3 A and C). Their fluorescence emissions are well maintained for 7 days of storage (Fig. 3 B and D). By contrast, conventional organic dyes are rapidly extinguished when exposed to outside lights. These unique features of QDs are particularly useful for biomedical labeling [17,36].

MR contrast agents are evaluated on the basis of their relaxivity or the change in the relaxation rates of water protons in the presence of the agent per unit concentration [37]. The MR relaxivity of the Gd^{3+} DTPA·BSA@QDs nanoparticles were measured using a 1.41 T MRI facility at 37 °C in water by measuring the longitudinal (r_1) and the transverse (r_2) nuclear magnetic relaxation rates of water protons. As shown in Fig. 4 A and B, Gd^{3+} DTPA·BSA and Gd^{3+} DTPA·BSA@QDs have high r_1 values of 15.357 and 16.561 s^{-1} per mM of Gd^{3+} respectively. These values are nearly fourfold that of commercially used Gd-DTPA. The significant improvement on relaxivity can be attributed to the BSA macromolecule binding, which can restrict Gd-DTPA rotation [38]. The r_2/r_1 ratio is a key factor to evaluate a given material for a preferable T_1 or T_2 contrast efficacy [39]. Remarkably low r_2/r_1 values of 1.57 and 1.67 of Gd^{3+} DTPA·BSA and Gd^{3+} DTPA·BSA@QDs are obtained, respectively, suggesting their ideal candidacy for T_1 -weighted MR contrast agents.

Fig. 4C shows three sets of Gd^{3+} DTPA·BSA@QDs with Gd^{3+} concentrations ranging from 0.15 to 0.46 mM that are imaged using T_1 -weighted spin-echo sequences. The intense signals of Gd^{3+} DTPA·BSA@QDs are clearly visualized at the highest concentration of Gd^{3+} (0.46 mM). Even at the lowest concentration of Gd^{3+} (0.15 mM), the signal of Gd^{3+} DTPA·BSA@QDs is much brighter than water. Their high r_1 value and excellent MRI enhancement capability show promise as a positive contrast agents.

3.3. Cytotoxicity study

3T3 cells were incubated with Gd^{3+} DTPA·BSA @QDs at different Cd^{2+} concentrations for 24 h, 48 h and 72 h. Their corresponding cell viability data obtained by MTT assay is shown in Fig. 5. As can be seen in this figure, after 24 h of incubation, more than 80% of 3T3 cells survived at all Cd^{2+} concentrations. In addition, no significant cytotoxicities are found for times up to 48 h and 72 h in the Cd^{2+} concentration ranging from 0.1 μ M to 100 μ M, suggesting its good biocompatibility with 3T3 cells at the given concentrations.

3.4. In vitro cellular fluorescent and MR targeted imaging

Human Colonic cancer cells (HCT116) were used *in vitro* to assess the biological specificity of the Gd^{3+} DTPA·BSA@QDs-PcAb nanoprobe. Proliferating HCT116 cells overexpress Glut1 surface protein [40]. HCT116 cells were incubated with Gd^{3+} DTPA·BSA@QDs-PcAb and Gd^{3+} DTPA·BSA@QDs respectively for 30 min. The CLSM images are shown in Fig. 6A. An intense red fluorescence is observed from the emission of Gd^{3+} DTPA·BSA@QDs-PcAb nanoprobe on the surface of HCT116, while CLSM images of HCT116 cells incubated with Gd^{3+} DTPA·BSA@QDs show no red fluorescence in the cell membranes. To verify the specificity of the Gd^{3+} DTPA·BSA@QDs-PcAb nanoprobe with the cells mainly driven by Glut1 receptor-mediated binding, competition experiments under the same experimental conditions was performed by conducting Gd^{3+} DTPA·BSA@QDs-PcAb nanoprobe incubation with cells in the presence of 10 mM free excess Glut1 antibodies. It is found that the pre-incubated cells with free antibodies are hardly labeled by Gd^{3+} DTPA·BSA@QDs-PcAb nanoprobe (Fig. 6 A). The fluorescence reduction is likely associated with excess free Glut1 antibodies bind to the surface receptors of HCT116 cancer cells, inhibiting surface cellular specific binding with the nanoprobe. These cellular assays results indicate the binding of Gd^{3+} DTPA·BSA@QDs-PcAb to HCT116 cells due to antigen–antibody reaction [15].

To exploit the full potentials of Gd^{3+} DTPA·BSA@QDs-PcAb as multipurpose nanoprobe, *in vitro* cellular MRI was performed. 3×10^6 HCT116 cells were respectively incubated with Gd^{3+} DTPA·BSA@QDs-PcAb and non-targeted Gd^{3+} DTPA·BSA@QDs, and without any contrast agent for 2 h at 37 °C. Fig. 6 B shows the bright red fluorescence image from cells incubated with the Gd^{3+} DTPA·BSA@QDs-PcAb nanoprobe. The cells incubated with Gd^{3+} DTPA·BSA@QDs and the control groups exhibit weak or no fluorescence. These cells were then MR scanned (Fig. 6C). It shows much brighter HCT116 cells incubated with Gd^{3+} DTPA·BSA@QDs-PcAb than those with Gd^{3+} DTPA·BSA@QDs, and the control blank cells. The T_1 relaxation time of HCT116 cells incubated with Gd^{3+} DTPA·BSA@QDs-PcAb is 311 ± 10.6 ms, much lower than those incubated with Gd^{3+} DTPA·BSA@QDs (643 ± 6.5 ms) and the blank control cells (665 ± 2.9 ms) (Fig. 6 D). These values are consistent with the results of CLSM images and MRI enhancement performance in Fig. 6A, B, C.

The distribution and expression of Glut1 of CRC cells are investigated by *in vitro* cellular confocal fluorescent imaging and MR scanning after treated with Gd^{3+} DTPA·BSA@QDs-PcAb. The *in vitro* CLSM and MR cellular imaging demonstrate significant

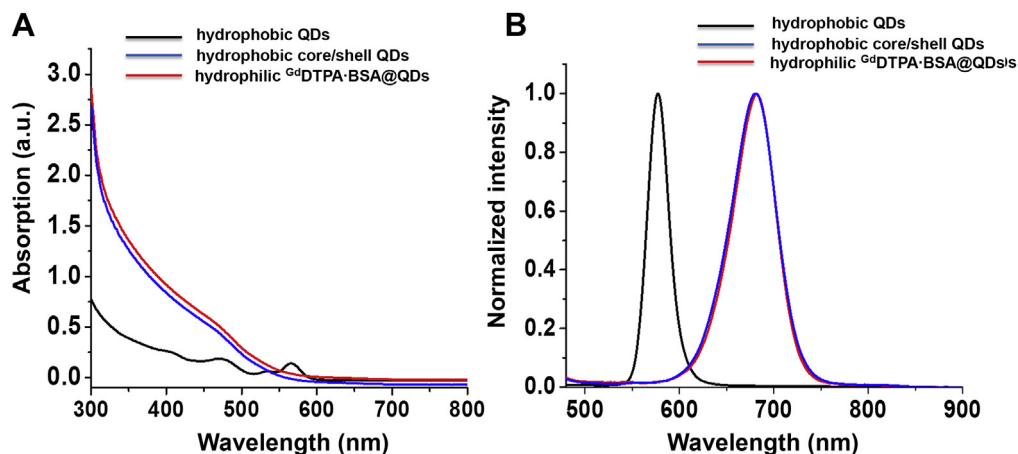


Fig. 2. UV–vis absorption (A) and PL emission (B) spectra of representative core/shell QDs before (blue) and after (red) phase transfer with use of Gd^{3+} DTPA·BSA. The core QDs is also shown in black. (For interpretation of the references to color in this figure legend, the reader is referred to the web version of this article.)

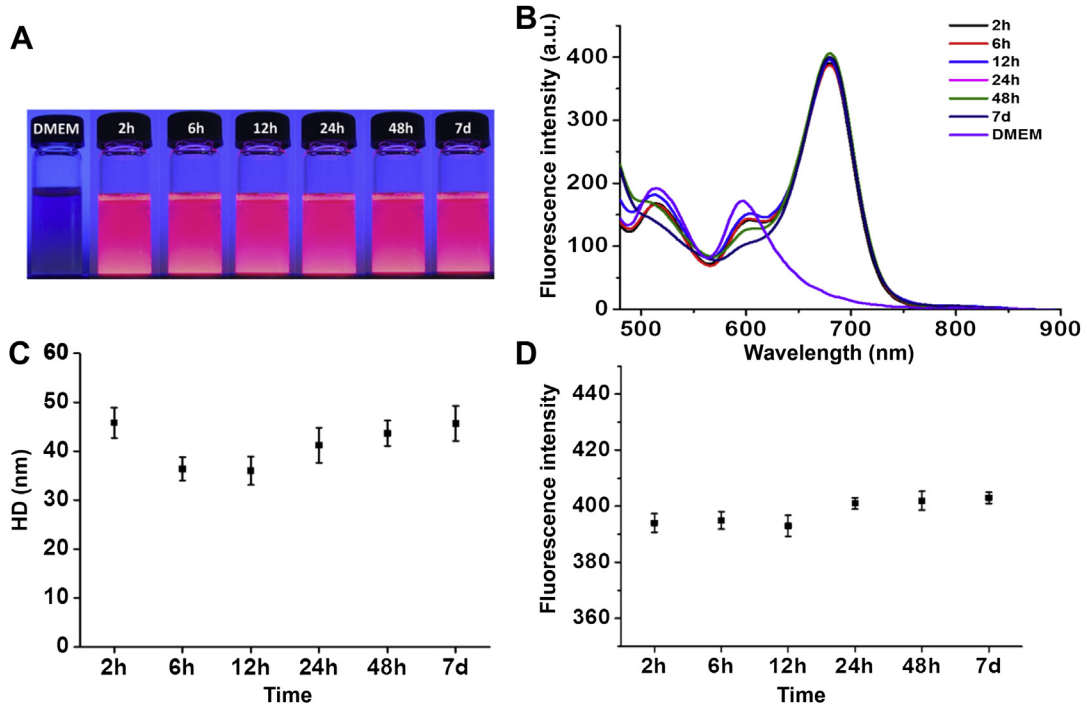


Fig. 3. (A) Digital luminescent images of $Gd^{DTPA}\cdot BSA@QDs$ emissions at DMEM solution after 7 days storage at room temperature excited with a hand-held UV lamp at 365 nm. Time-resolved fluorescent quantitative and hydrodynamic diameter evaluation of $Gd^{DTPA}\cdot BSA@QDs$ (B, C and D) at DMEM solution recorded at room temperature at various time points.

specific binding of Glut1-targeted $Gd^{DTPA}\cdot BSA@QDs\text{-PcAb}$ to HCT116 cells but not of those non-targeted $Gd^{DTPA}\cdot BSA@QDs$.

3.5. *In vivo* tumor targeted MRI

Both $Gd^{DTPA}\cdot BSA@QDs$ and $Gd^{DTPA}\cdot BSA@QDs\text{-PcAb}$ were estimated for targeting behaviors in tumor accumulation *in vivo* by MRI. Fig. 7 shows antibody-linked nanoprobe specifically captured

in the lesion of tumor, leading to enhanced MRI for diagnosis. This active targeting to the colorectal tumor was found as fast as 30 min post-injection. The tumor enhancement reached its maximum value at 240 min post-injection (Fig. 7 A), while T_1 -weighted MR images obtained at $t = 0$ to $t = 480$ min for the mouse injected with non-targeted $Gd^{DTPA}\cdot BSA@QDs$ show no or little contrast enhancement in the tumor area (Fig. 7 B). These results show effective targeting of $Gd^{DTPA}\cdot BSA@QDs\text{-PcAb}$ to colorectal tumor

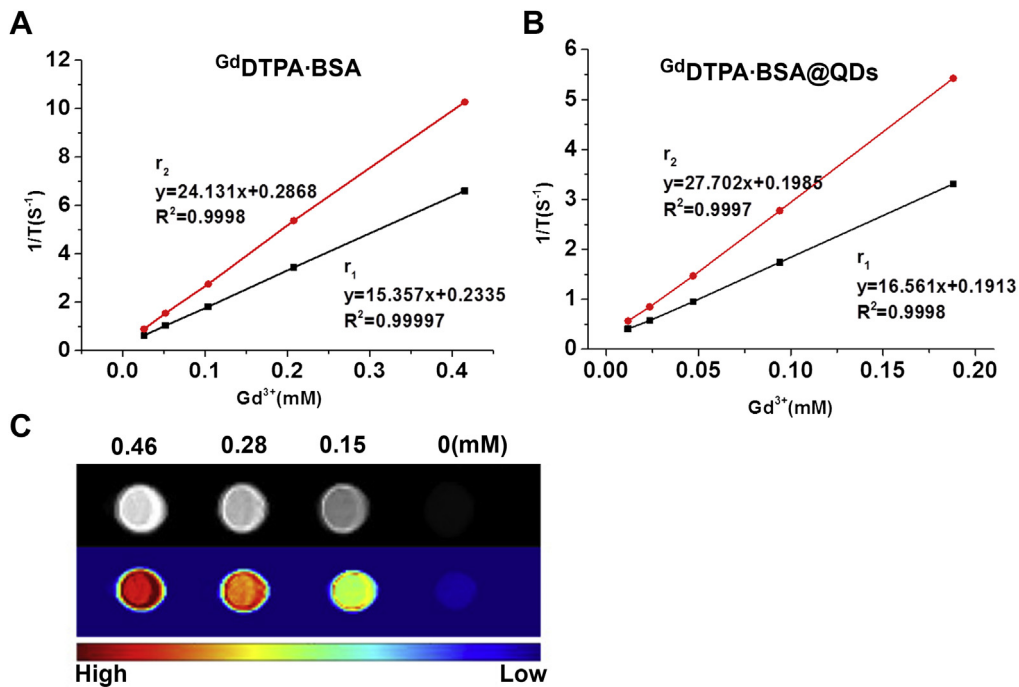


Fig. 4. T_1 relaxation rates ($1/T_1$) and T_2 relaxation rates ($1/T_2$) of $Gd^{DTPA}\cdot BSA$ (A) and $Gd^{DTPA}\cdot BSA@QDs$ (B) in aqueous solution (37 °C) as a function of Gd^{3+} concentration. (C) T_1 -weighted MR images of $Gd^{DTPA}\cdot BSA@QDs$ with different Gd^{3+} concentrations. Deionized water (0 mM) is used as the reference.

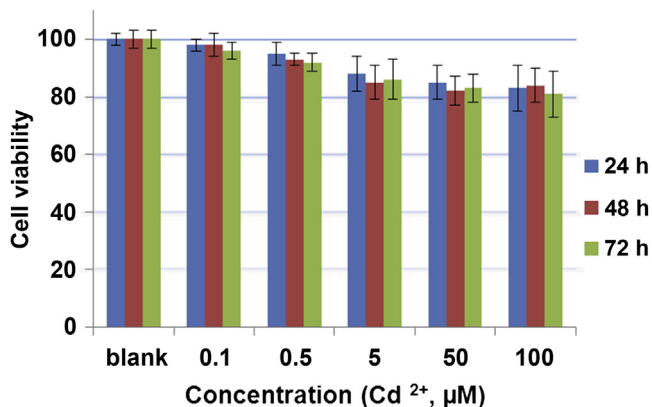


Fig. 5. Cytotoxicities of $GdDTPA\cdot BSA@QDs$ with different Cd^{2+} concentrations to 3T3 cells were determined by the MTT cell proliferation assay. The results are obtained from five experiments with standard deviations.

by conjugating the polyclonal anti-Glut1 antibody with high specificity *via* receptor-mediated reaction, providing contrast enhanced MRI *in vivo*.

In vivo MRI shows strong positive signals in the CRC tumor area which distinguishes the boundary between the tumor and normal

tissues and provides impressive anatomic resolution. These results show a promising candidate of the $GdDTPA\cdot BSA@QDs-PcAb$ nanoprobes for the CRC contrast-enhanced MRI diagnosis.

3.6. IHC analysis on biopsy tissue specimens

In vivo MRI shows real-time imaging of CRC tumor on nude mice after intravenously injection of $GdDTPA\cdot BSA@QDs-PcAb$. *Ex vivo* immunofluorescent molecular imaging on the biopsy tissue were subsequently conducted and confirmed for the expression of Glut1. Fig. 8 shows intense red fluorescence in the targeted group (B), but no fluorescence signals in the non-targeted group (F). These results are consistent with the enzyme-based IHC data on tumor tissues in both groups (Fig. 8 A, E). The cell nuclei were stained with DAPI for locating the nanoprobes in the involved cells (Fig. 8C, G). Strong red fluorescence signals in the targeted group are observed on the cell membranes (Fig. 8 D, H), which further confirms the specific binding of $GdDTPA\cdot BSA@QDs-PcAb$ with cells mediated by Glut1. The Glut 1 expressions are imaged on the *in vitro* cells, *in situ* tumor lesion and *ex vivo* biopsy tissue specimens. The $GdDTPA\cdot BSA@QDs-PcAb$ nanoprobes are shown to be capable of imaging Glut 1 at various biological levels. The so-called “imaging-biopsy” reconfirmation strategy can provide accurate diagnosis.

In clinical applications, as a critical step in conclusive cancer diagnosis, the corroborative evidence must be provided other than

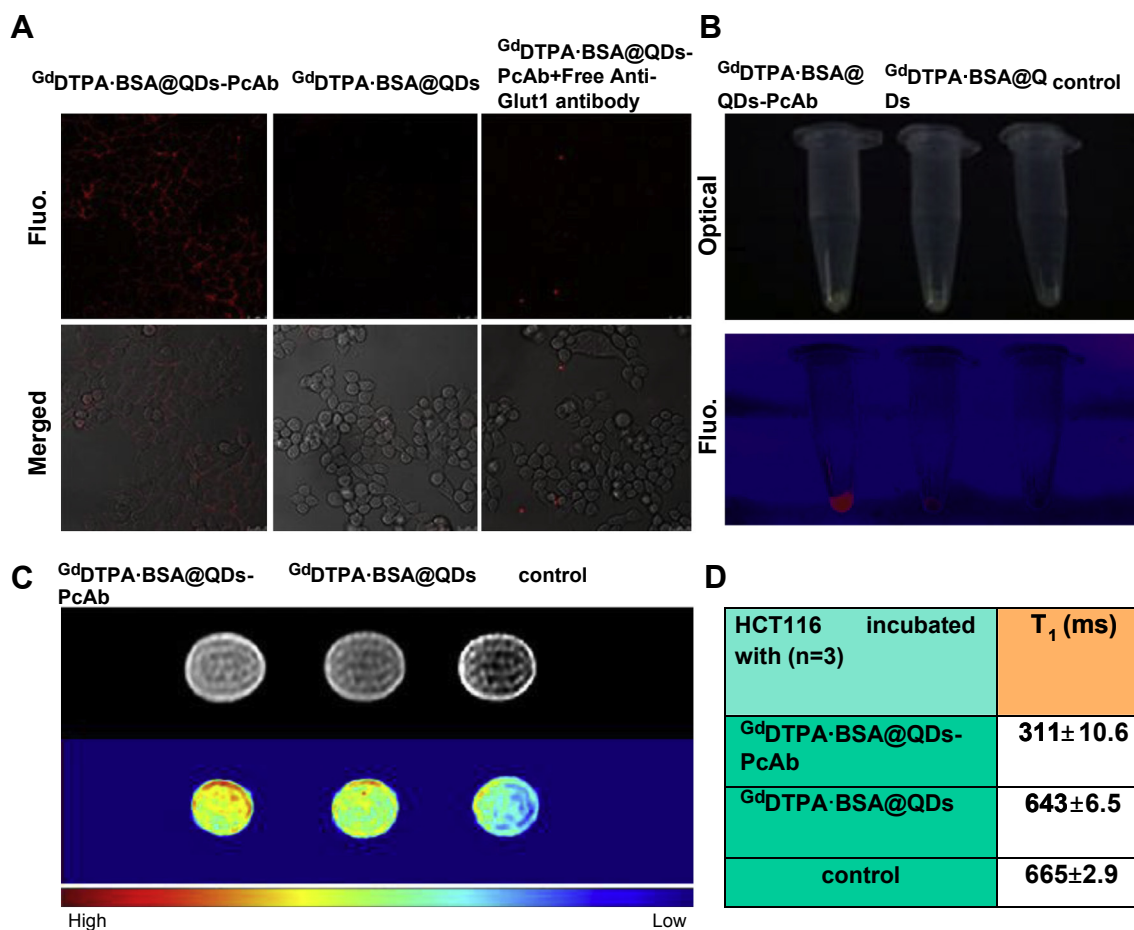


Fig. 6. (A) CLSM images of HCT116 cells incubated with Glut1-targeted $GdDTPA\cdot BSA@QDs-PcAb$ and non-targeted $GdDTPA\cdot BSA@QDs$ for 30 min. To further determine targeting specificity, cells were preincubated with free Glut1 antibodies before adding Glut1-targeted $GdDTPA\cdot BSA@QDs-PcAb$ nanoprobes. (B) Photograph under white light and an excitation with a hand-held UV lamp at 365 nm, T₁-weighted MRI image (C), and the T₁ relaxation times (D) for HCT116 cells incubated with Glut1-targeted $GdDTPA\cdot BSA@QDs-PcAb$ and non-targeted $GdDTPA\cdot BSA@QDs$, and without any contrast agent for 2 h.

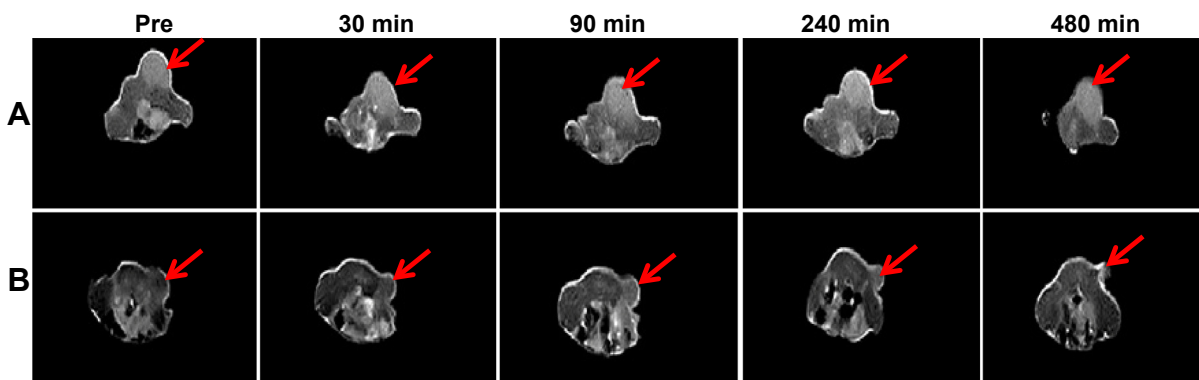


Fig. 7. *In vivo* CRC tumor-bearing MRI. T₁-weighted MRI of nude mice intravenously injected with targeted ^{Gd}DTPA·BSA@QDs-PcAb nanoprobe (A), and non-targeted ^{Gd}DTPA·BSA@QDs (B). Images were collected at different time points: pre injection, 30 min, 90 min, 240 min, and 480 min post-injection.

the imaging techniques. A biopsy is a medical test commonly performed by a surgeon or an interventional radiologist involving sampling of cells or tissues for pathological examination. In this study, the tumor tissue was extracted by biopsy to further study the expression of Glut1 in the tumor tissue. ^{Gd}DTPA·BSA@QDs-PcAb nanoprobes can provide a potential immunofluorescence solution in labeling the specific proteins on the biopsy tissue specimens (Fig. 8). As shown in Fig. 8, the ^{Gd}DTPA·BSA@QDs-PcAb based IHC data shows good correlation and consistency with the conventional enzyme-based IHC.

In this study, the ^{Gd}DTPA·BSA@QDs-PcAb nanoprobes have been utilized for both *in vivo* imaging and subsequent biopsy tissue analysis. The proof-of-concept study may extend the nanoprobes designed in this study in many clinical applications including imaging contrast agents, early diagnosis of cancers, and biopsy tissue analysis.

3.7. Biodistribution study and histology toxicity analysis

To evaluate the *in vivo* clearance process and organ distribution, mice were injected with the ^{Gd}DTPA·BSA@QDs nanoparticles via

tail vein and then sacrificed at different time points. The main organs were removed for ICP-AES quantitative analysis of Cd²⁺ and Gd³⁺ by ICP-AES (Fig. 9). ICP analysis shows uptake and retention of ^{Gd}DTPA·BSA@QDs nanoparticles mainly in liver, while negligible amounts of gadolinium and cadmium in heart and lung. ICP analysis also reveals a gradual decrease in liver, suggesting that the ^{Gd}DTPA·BSA@QDs nanoparticles may take a biliary elimination pathway. The injected nanoparticles with size of 35 nm cannot be primarily cleared out by glomerular filtration. Therefore, a thimbleful of Gd³⁺ and Cd²⁺ were present in kidneys post-injection. Previous studies showed large particles were more easily captured by liver and the RES system [41,42]. In this study, biodistribution study shows that the clearance route of the ^{Gd}DTPA·BSA@QDs nanoparticles is mainly via hepatobiliary excretion.

A histological analysis of organs was performed to determine possible damage of tissue, inflammation, or lesions by ^{Gd}DTPA·BSA@QDs (Fig. 10). QDs used in this study contain heavy metal cadmium constituents [43]. Exposure to Cd²⁺ could induce degenerative changes in the organs [44,45]. Liver, spleen and kidney were chosen for the *in vivo* toxicity test since they retained

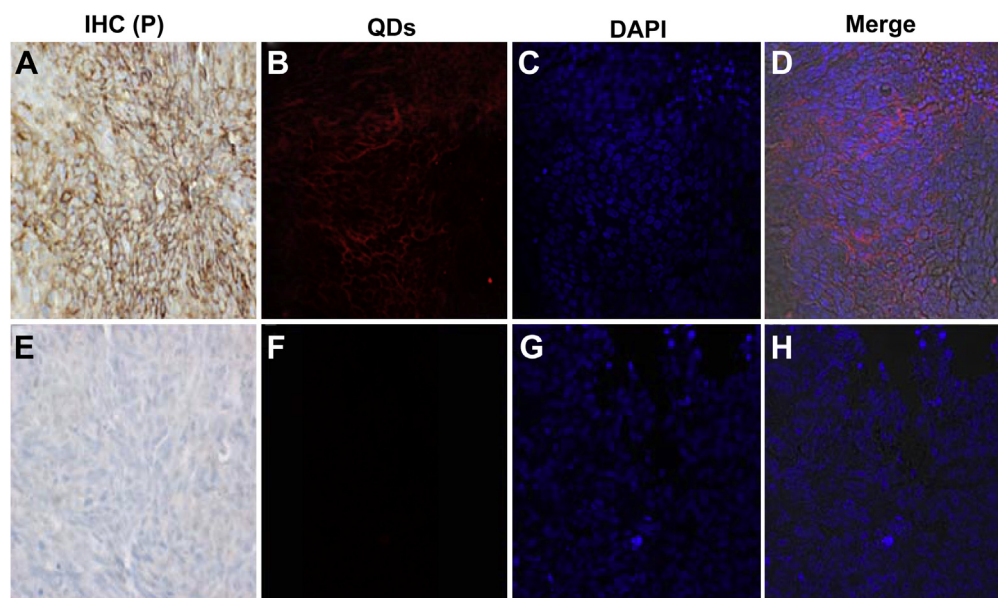


Fig. 8. Examination of Glut1 expression by IHC analysis. (A) Glut1 IHC of colon carcinomas with enzyme-labeled IgG as the reporter. (B) Glut1 IHC of colon carcinomas with ^{Gd}DTPA·BSA@QDs-PcAb nanoprobes as the reporter. Cell nuclei were stained with DAPI (C, G) and merged images are shown (D, H). In the control experiments, primary Glut1 antibodies were not added (E) and non-targeted ^{Gd}DTPA·BSA@QDs were used (F).

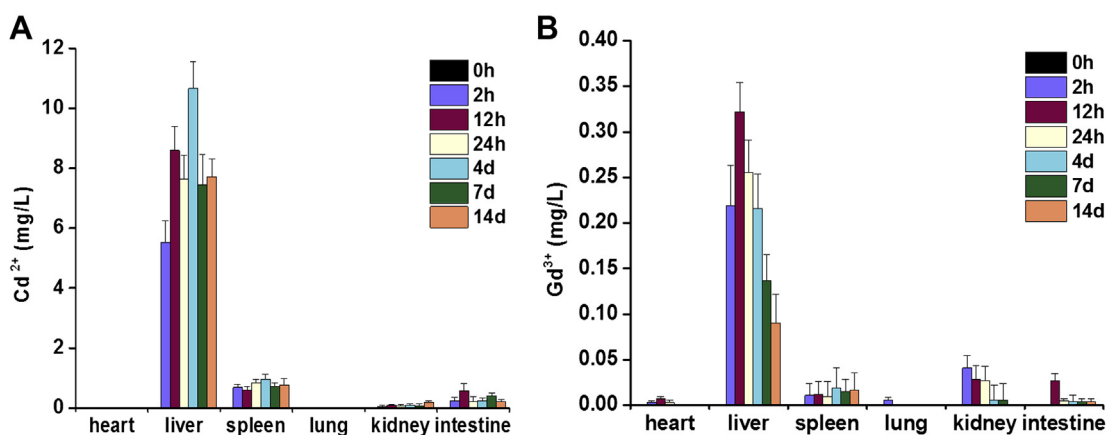


Fig. 9. Biodistribution of $GdDTPA \cdot BSA@QDs$ in mice. ICP-AES histograms of cadmium ions (A) and gadolinium ions (B) in heart, liver, spleen, lung, kidney, and intestine of the control mice and the mice sacrificed 2 h, 12 h, 24 h and 4 d, 7 d and 14 d post-injection with $GdDTPA \cdot BSA@QDs$ ($n = 3$).

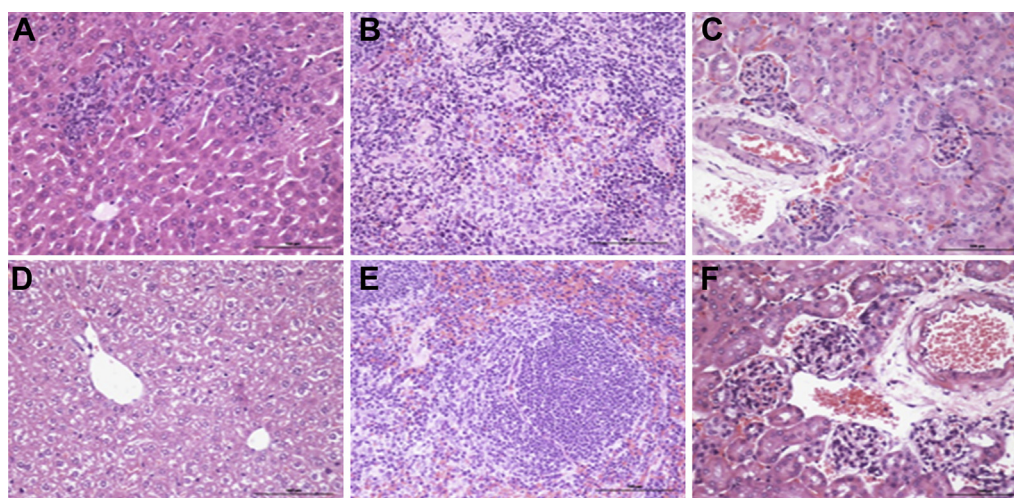


Fig. 10. Hematoxylin and eosin-stained tissue sections from mice injected with $GdDTPA \cdot BSA@QDs$ 15 days post-injection (A, B, and C) and no injection (D, E, and F). Tissues were harvested from liver (A, D), spleen (B, E), and kidney (C, F).

most of the injected nanoparticles (Fig. 9). All investigated organs of the experimental mice were found normal, preserving the same structures as those of the control group as shown in Fig. 10. Typically, the cytoplasm appeared light, the chromatin became condensed, and the intercellular space began to enlarge in many hepatocytes. Many circumambient hepatic sinusoids were also infiltrated by numerous Kupffer cells or NK cells. No nucleus fragmentation was found in the liver cells. The kidney morphology of the $GdDTPA \cdot BSA@QDs$ group remained the same compared to the control animals. Locally, lymphocyte infiltrates were observed in spleen, most frequently in the renal parenchymal cells. No necrosis and bleeding were found in any of the groups. Only slight histological changes were observed but no obvious toxicity in the liver, kidney and spleen groups.

4. Conclusions

In summary, CRC is diagnosed at the levels of *in vitro* cellular assay, *in vivo* solid tumor MRI, and *ex vivo* tissue biopsy analysis, by using the $GdDTPA \cdot BSA@QDs$ -PcAb nanoprobe. These multipurpose $GdDTPA \cdot BSA@QDs$ -PcAb nanoprobe are synthesized by surface engineering of QDs with DTPA-BSA- Gd^{3+} macromolecule complex under ultrasonication condition. The resulting $GdDTPA \cdot BSA@QDs$

exhibit excellent colloidal stability with fine hydrodynamic size in a wide range of pH and ionic strength values. They exhibit much higher longitudinal relaxivity and transverse relaxivity in water than those commercial Gd -DTPA solutions. $GdDTPA \cdot BSA@QDs$ labeled with polyclone antibodies present cell-targeted imaging. *In vivo* MRI shows a promising candidate of $GdDTPA \cdot BSA@QDs$ -PcAb for CRC contrast-enhanced MRI diagnosis. In particular, $GdDTPA \cdot BSA@QDs$ -PcAb can also be utilized for tumor biopsy tissue specimen analysis. Biodistribution results indicate gradual clearance of the nanoprobe from body *via* hepatobiliary excretion. No obvious toxicity is found by *in vitro* MTT assay and *in vivo* toxicity studies. Based on the extensive experimental results of this study, the $GdDTPA \cdot BSA@QDs$ -PcAb nanoprobe has shown great potential in CRC tumor-targeted MRI and tumor tissue biopsy analysis.

Acknowledgments

This work was partially supported by the National Natural Science Foundation of China (81371618), the Program of Science and Technology Commission of Shanghai Municipal (No. 10411953500), Shanghai Innovation Program (14ZZ039), the Program of Science and Technology Commission of Shanghai Municipal for young scientists (13ZR1459400), the new hundred people program of the

board of health (03.02.11015), Program for Outstanding Young Teachers in Tongji University, and the Fundamental Research Funds for the Central Universities.

References

- [1] Jemal A, Bray F, Center MM, Ferlay J, Ward E, Forman D. Global cancer statistics. *CA: A Cancer J Clin* 2011;61:69–90.
- [2] O'Connell JB, Maggard MA, Ko CY. Colon cancer survival rates with the new American Joint Committee on Cancer sixth edition staging. *J Natl Cancer Inst* 2004;96:1420–5.
- [3] Amann T, Maegdefrau U, Hartmann A, Agaimy A, Marienhagen J, Weiss TS, et al. GLUT1 expression is increased in hepatocellular carcinoma and promotes tumorigenesis. *Am J Pathol* 2009;174:1544–52.
- [4] Shim BY, Jung JH, Lee KM, Kim HJ, Hong SH, Kim SH, et al. Glucose transporter 1 (GLUT1) of anaerobic glycolysis as predictive and prognostic values in neoadjuvant chemoradiotherapy and laparoscopic surgery for locally advanced rectal cancer. *Int J Colorectal Dis* 2013;28:375–83.
- [5] Koukourakis MI, Giatromanolaki A, Polychronidis A, Simopoulos C, Gatter KC, Harris AL, et al. Endogenous markers of hypoxia/anaerobic metabolism and anemia in primary colorectal cancer. *Cancer Sci* 2006;97:582–8.
- [6] Younes M, Lechago LV, Lechago J. Overexpression of the human erythrocyte glucose transporter occurs as a late event in human colorectal carcinogenesis and is associated with an increased incidence of lymph node metastases. *Clin Cancer Res* 1996;2:1151–4.
- [7] Haber RS, Rathana A, Weiser KR, Pritsker A, Itzkowitz SH, Bodian C, et al. Glut1 glucose transporter expression in colorectal carcinoma. *Cancer* 1998;83:34–40.
- [8] Sakashita M, Aoyama N, Minami R, Maekawa S, Kuroda K, Shirasaka D, et al. Glut1 expression in T1 and T2 stage colorectal carcinomas: its relationship to clinicopathological features. *Eur J Cancer* 2001;37:204–9.
- [9] Winciewicz A, Sulkowski M, Koda M. Clinicopathological significance and linkage of the distribution of HIF-1 α and GLUT-1 in human primary colorectal cancer. *Pathol Oncol Res* 2007;13:15–20.
- [10] Fenske W, Völker H-U, Adam P, Hahner S, Johanssen S, Wortmann S, et al. Glucose transporter GLUT1 expression is a stage-independent predictor of clinical outcome in adrenocortical carcinoma. *Endocrine-Related Cancer* 2009;16:919–28.
- [11] Stasiuk GJ, Tamang S, Imbert D, Poillot C, Giardiello M, Tisseyre C, et al. Cell-permeable Ln (III) chelate-functionalized InP quantum dots as multimodal imaging agents. *ACS Nano* 2011;5:8193–201.
- [12] Longmire M, Choyke PL, Kobayashi H. Dendrimer-based contrast agents for bioimaging. *Curr Top Med Chem* 2008;8:1180–6.
- [13] Huang CH, Tsourkas A. Gd-based macromolecules and nanoparticles as magnetic resonance contrast agents for molecular imaging. *Curr Top Med Chem* 2013;13:411–21.
- [14] Drevs J, Schneider V. The use of vascular biomarkers and imaging studies in the early clinical development of anti-tumour agents targeting angiogenesis. *J Intern Med* 2006;260:517–29.
- [15] Airley R, Evans A, Mobasher A, Hewitt SM. Glucose transporter Glut-1 is detectable in peri-necrotic regions in many human tumor types but not normal tissues: study using tissue microarrays. *Ann Anatomy-Anatomischer Anzeiger* 2010;192:133–8.
- [16] Younes M, Lechago LV, Somoano JR, Mosharaf M, Lechago J. Wide expression of the human erythrocyte glucose transporter Glut1 in human cancers. *Cancer Res* 1996;56:1164–7.
- [17] Zrazhevskiy P, Sena M, Gao X. Designing multifunctional quantum dots for bioimaging, detection, and drug delivery. *Chem Soc Rev* 2010;39:4326–54.
- [18] Michalet X, Pinaud FF, Bentolila LA, Tsay JM, Doose S, Li JJ, et al. Quantum dots for live cells, in vivo imaging, and diagnostics. *Science* 2005;307:538–44.
- [19] Diagaradjane P, Deorukhkar A, Gelovani JG, Maru DM, Krishnan S. Gadolinium chloride augments tumor-specific imaging of targeted quantum dots in vivo. *ACS Nano* 2010;4:4131–41.
- [20] Chen C, Peng J, Sun S-R, Peng C-W, Li Y, Pang D-W. Tapping the potential of quantum dots for personalized oncology: current status and future perspectives. *Nanomedicine* 2012;7:411–28.
- [21] Xing Y, Chaudry Q, Shen C, Kong KY, Zhou HE, Chung LW, et al. Bioconjugated quantum dots for multiplexed and quantitative immunohistochemistry. *Nat Protoc* 2007;2:1152–65.
- [22] Zlateva G, Zhelev Z, Bakalova R, Kanno I. Precise size control and synchronized synthesis of six colors of CdSe quantum dots in a slow-increasing temperature gradient. *Inorg Chem* 2007;46:6212–4.
- [23] Peng ZA, Peng X. Formation of high-quality CdTe, CdSe, and CdS nanocrystals using CdO as precursor. *J Am Chem Soc* 2001;123:183–4.
- [24] Zhang B, Wang X, Liu F, Cheng Y, Shi D. Effective reduction of nonspecific binding by surface engineering of quantum dots with bovine serum albumin for cell-targeted imaging. *Langmuir* 2012;28:16605–13.
- [25] de Wit M, Jimenez CR, Carvalho B, Belien JA, Delis-van Diemen PM, Mongera S, et al. Cell surface proteomics identifies glucose transporter type 1 and prion protein as candidate biomarkers for colorectal adenoma-to-carcinoma progression. *Gut* 2012;61:855–64.
- [26] Li JJ, Wang YA, Guo W, Keay JC, Mishima TD, Johnson MB, et al. Large-scale synthesis of nearly monodisperse CdSe/CdS core/shell nanocrystals using air-stable reagents via successive ion layer adsorption and reaction. *J Am Chem Soc* 2003;125:12567–75.
- [27] Li S, He H, Cui W, Gu B, Li J, Qi Z, et al. Detection of A β plaques by a novel specific MRI probe precursor CR-BSA-(Gd-DTPA) n in APP/PS1 transgenic mice. *Anat Rec* 2010;293:2136–43.
- [28] Mandeville JS, Tajmir-Riahi HA. Complexes of dendrimers with bovine serum albumin. *Biomacromolecules* 2010;11:465–72.
- [29] Schmiedl U, Ogan M, Paajanen H, Marotti M, Crooks LE, Brito AC, et al. Albumin labeled with Gd-DTPA as an intravascular, blood pool-enhancing agent for MR imaging: biodistribution and imaging studies. *Radiology* 1987;162:205–10.
- [30] Wakayama J, Sekiguchi H, Akanuma S, Ohtani T, Sugiyama S. Methods for reducing nonspecific interaction in antibody-antigen assay via atomic force microscopy. *Anal Biochem* 2008;380:51–8.
- [31] Yang B, Wyman CE. BSA treatment to enhance enzymatic hydrolysis of cellulose in lignin containing substrates. *Biotechnol Bioeng* 2006;94:611–7.
- [32] Wang X, Xing X, Zhang B, Liu F, Cheng Y, Shi D. Surface engineered antifouling optomagnetic SPIONs for bimodal targeted imaging of pancreatic cancer cells. *Int J Nanomed* 2014;9:1601–15.
- [33] Chen J, Tao X, Zhang M, Sun A, Zhao L. Properties and stability of blueberry anthocyanin – bovine serum albumin nanoparticles. *J Sci Food Agric* 2014;94:1781–6.
- [34] Sun SK, Dong LX, Cao Y, Sun HR, Yan XP. Fabrication of multifunctional Gd2O3/Au hybrid nanoprobe via a one-step approach for near-infrared fluorescence and magnetic resonance multimodal imaging in vivo. *Anal Chem* 2013;85:8436–41.
- [35] Zhang BB, Jin HT, Li Y, Chen BD, Liu SY, Shi DL. Bioinspired synthesis of gadolinium-based hybrid nanoparticles as MRI blood pool contrast agents with high relaxivity. *J Mater Chem* 2012;22:14494–501.
- [36] Shah BS, Mao JJ. Labeling of mesenchymal stem cells with bioconjugated quantum dots. *Methods Mol Biol* 2011;680:61–75.
- [37] Hu F, MacRenaris KW, Waters EA, Liang T, Schultz-Sikma EA, Eckermann AL, et al. Ultrasmall, water-soluble magnetite nanoparticles with high relaxivity for magnetic resonance imaging. *J Phys Chem C* 2009;113:20855–60.
- [38] Schmiedl UOM, Moseley ME, Brasch RC. Comparison of the contrast-enhancing properties of albumin-(Gd-DTPA) and Gd-DTPA at 2.0 T: and experimental study in rats. *AJR Am J Roentgenol* 1986;147:1263–70.
- [39] Kim BH, Lee N, Kim H, An K, Park YI, Choi Y, et al. Large-scale synthesis of uniform and extremely small-sized iron oxide nanoparticles for high-resolution T1 magnetic resonance imaging contrast agents. *J Am Chem Soc* 2011;133:12624–31.
- [40] Kurokawa T, Yoshida Y, Kawahara K, Tsuchida T, Okazawa H, Fujibayashi Y, et al. Expression of GLUT-1 glucose transfer, cellular proliferation activity and grade of tumor correlate with [F-18]-fluorodeoxyglucose uptake by positron emission tomography in epithelial tumors of the ovary. *Int J Cancer* 2004;109:926–32.
- [41] Souris JS, Lee C-H, Cheng S-H, Chen C-T, Yang C-S, J-a Ho, et al. Surface charge-mediated rapid hepatobiliary excretion of mesoporous silica nanoparticles. *Biomaterials* 2010;31:5564–74.
- [42] Longmire M, Choyke PL, Kobayashi H. Clearance properties of nano-sized particles and molecules as imaging agents: considerations and caveats. *Nanomedicine (London, England)* 2008;3:703–17.
- [43] Godt J, Scheidig F, Grosse-Siestrup C, Esche V, Brandenburg P, Reich A, et al. The toxicity of cadmium and resulting hazards for human health. *J Occup Med Toxicol* 2006;1:1–6.
- [44] Kirchner C, Liedl T, Kudera S, Pellegrino T, Javier AM, Gaub HE, et al. Cytotoxicity of colloidal CdSe and CdSe/ZnS nanoparticles. *Nano Lett* 2005;5:331–8.
- [45] Shiohara A, Hoshino A, Hanaki K, Suzuki K, Yamamoto K. On the cyto-toxicity caused by quantum dots. *Microbiol Immunol* 2004;48:669–75.